Supermolecular switches based on multiwalled carbon nanotubes

A. Subramanian,[1,a)] L. X. Dong,[1,b)] B. J. Nelson,[1,c)] and A. Ferreira[2]
[1]*Institute of Robotics and Intelligent Systems, ETH Zurich, 8092 Zurich, Switzerland*
[2]*Institut PRISME, ENSI Bourges, 88 Boulevard Lahitolle, 18000 Bourges, France*

(Received 11 December 2009; accepted 27 January 2010; published online 19 February 2010)

Electrostatically actuated nanoelectromechanical switches based on intershell displacement mechanisms within batch fabricated, bidirectional multiwalled carbon nanotube (MWNT) bearings are reported. Multiple devices with a 220 nm pitch are constructed within individual MWNT supermolecules. Experimental results on performance metrics including low switching voltages (0.8 to 6 V), repeatability, hysteresis, and failure modes are presented. © *2010 American Institute of Physics*. [doi:10.1063/1.3327514]

Arc-grown multiwalled carbon nanotubes (MWNTs) represent a physical realization of ideal building blocks for nanoelectromechanical systems (NEMS). Suitable modification of the as-grown, nested-shell MWNT architecture makes it possible to slide[1,2] and rotate[3] individual nanotube shells with respect to each other. The high-speed, low friction, low fatigue, and low wear characteristics of these linear/rotary nanobearings have been exploited to create nanomotors[3–5] and nanoresonators.[6,7] Electromechanical switches, relays, memories, and logic elements represent another important family of devices that can be realized using telescoping nanobearings.[8–13] These devices compare favorably with other technologies in terms of size, power consumption, and speed (estimated to be in the gigahertz regime). However, investigations of these electrostatically actuated telescoping devices has primarily been confined to theoretical studies,[8–12] and to date there has only been one experimental demonstration of this mechanism.[13]

Recently, we presented a hybrid nanofabrication process to fabricate multiple, but spatially separated, capless nanotube segments from a single MWNT.[14] In this paper, we present electrostatically actuated NEMS switches using this construct, which represents an operational demonstration of a bidirectional nanobearing architecture (unidirectional constructs reported previously included in Refs. 1, 2, and 13). Furthermore, our switches based on ultrasmall bearings (~200 nm length) demonstrate lower actuation voltages (0.8 to 6 V) as compared to those in Ref. 13 (where a third of the devices switched below 10 V). We also present insights into the repeatability, hysteresis and failure modes of these devices. The hybrid batch fabrication paradigm enables the construction of multiple switches (up to four demonstrated here) within a single MWNT at high densities (220 nm pitch), and improves on previous efforts that have constructed arc-grown, MWNT-based devices one at a time either by nanorobotic manipulation[5,6] or by surface micromachining structures at randomly dispersed NT sites on Si chips.[3,4]

The key aspects of the nanostructure illustrated in Fig. 1(a) include the following: (1) Dielectrophoretic (DEP) assembly of a MWNT onto five spatially separated electrodes. The electrodes are designed with a 220 nm pitch. (2) Piece-

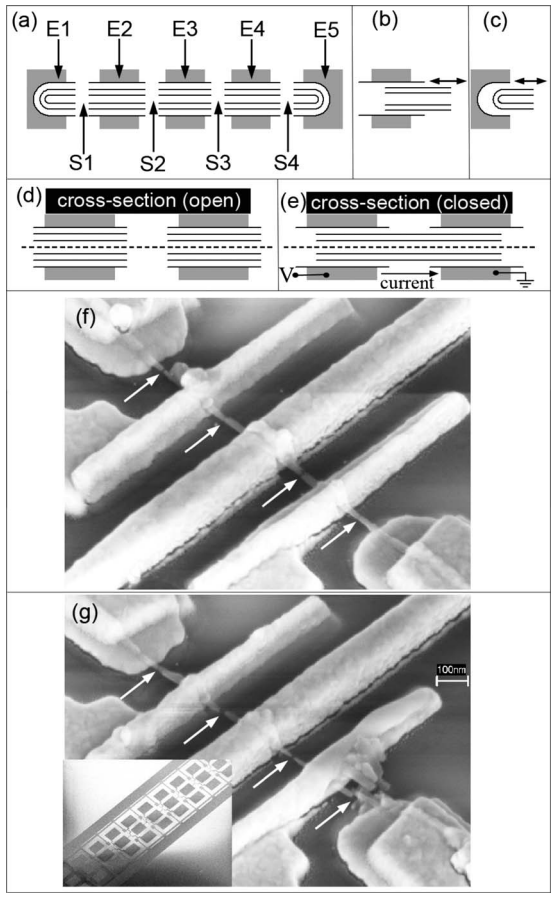

FIG. 1. Supermolecular switches based on bidirectional linear bearings. (a) A piecewise engineered MWNT bridging five spatially separated electrodes. The NT is engineered to create gaps in each of the suspended, interelectrode segments. The labeling terminology for electrodes ("E1" through "E5") and switches ("S1" through "S4") that would be used within this report are highlighted here. (b) Bidirectional shell architecture at electrodes "E2," "E3," and "E4." (c) The shell architecture at electrodes "E1" and "E5" showing the unidirectional nature of bearings at these locations. (d) Cross-sectional view of a switch in the "OFF" state. (e) Cross-sectional view of a switch in the "ON" state when an excitation bias beyond the characteristic threshold is applied. (f) SEM image (taken with a stage tilt of 40°) of multiple bidirectional bearings constructed within a MWNT using current induced shell etching. The arrows point to gaps engineered at each of the suspended, interelectrode NT segments. (g) Another MWNT nanostructure with the array design shown in inset. Scale bar represents 100 nm. Image in panel "f" has been reproduced from Ref. 14 with permission from IOP Publishing Ltd., Bristol, U.K.

[a)]Present address: Center for Integrated Nanotechnology, Sandia National Laboratories, Albuquerque, NM 87185. Electronic mail: asubram@sandia.gov.
[b)]Present address: Department of Electrical and Computer Engineering, Michigan State University, East Lansing, MI 48824.
[c)]Electronic mail: bnelson@ethz.ch.

wise, current-induced shell engineering[14,15] of the NT to create ~6 to 15 nm wide breaks in each of the four interelectrode NT segments that are suspended in air; (3) The three inner electrodes [labeled "E2" through "E4" in Fig. 1(a)] have an open, capless NT segment that is anchored at the outermost shell. As shown in the cross-sectional schematic of these NT segments [Fig. 1(b)], the inner shells are free to slide axially within the outer housing in either direction, and (4) at the distal electrodes, the NT caps and the metal electrode constrain the core to axially displace in only one direction, as shown in Fig. 1(c).

The operating principle of the multiple-device configuration contained within a MWNT is illustrated in Figs. 1(d) and 1(e). Each pair of spatially separated, opposing nanotube segments located between adjacent metal electrodes constitute a switching device [labeled "S1" through "S4" in Fig. 1(a)]. In the as-fabricated configuration, all four switches are in the "OFF" state. When a potential difference is applied between any two adjacent metallic contacts, charges with opposing polarities are induced in the respective nanotube segments. This results in two following types of electrostatic forces: (1) an intrasegment repulsive force (due to like charges) that extrudes the core from the outer housing, and (2) an intersegment attractive force (due to charges with opposing polarities) that causes the core shells within neighboring NT segments to move toward each other. Beyond a characteristic threshold bias, the combined contributions of these two electrostatic force components becomes higher than the van der Waals interactions within each of the two segments, and results in a closure of the gap [Fig. 1(e)]. In this "ON" state, a current flow is established between the metallic contacts.

The batch fabrication process[14] employed to construct these devices is as follows. Silicon chips with a 500 nm thick insulating oxide layer on top serve as the substrate. We define a lower layer of electrodes (15 nm Cr/45 nm Au) using a combination of electron-beam lithography (EBL) and lift-off. Next, MWNTs are assembled onto the nanoelectrodes from a suspension in ethanol using DEP. We employ a composite-field DEP bias [with a 3.2V ac (peak-to-peak) and 0.4V dc signal] for 120 s. To ensure robust electrical and mechanical contact to the NTs, we define a top metallic layer comprising of 15 nm Cr/45 nm Au, again using EBL and lift-off. Finally, we employ the current-driven breakdown technique to create nanoscale gaps in each of the interelectrode, suspended NT segments. In our process, we have observed single NT assembly yields of the order of 40%. This is primarily limited by suspension in-homogeneity, which can be improved with the use of centrifugation in combination with ultrasonication (the use of surfactants is an alternate option but it negatively impacts on NT conductivity/contact resistance). Detailed information on the fabrication procedure can be found in Ref. 14. Scanning electron microscopy (SEM) images of fabricated NEMS switches are shown in Figs. 1(f) and 1(g), and a section of the nanoarray design is shown in inset of panel "g." From these images taken with a stage tilt, it is evident that the NT segments are fully suspended in air in the interelectrode region. In addition, it can be seen that the shell-engineered gaps are located at the mid-lengths of NT segments between electrodes. Altering the location of these etched gaps from NT mid-lengths would enable ultraprecise engineering of bearing lengths. This can potentially be achieved by using nanomachined

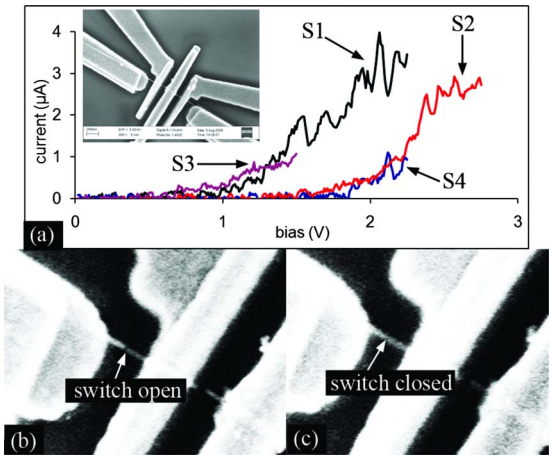

FIG. 2. (Color online) Switching results. (a) I-V plots of switches with low turn-on bias (0.8 to 2 V in this case). The engineered NT is shown in inset. [(b) and (c)] SEM images of a device in the open and closed configurations.

heat sinks across the NT to control the Joule-heat induced temperature distribution.[16]

During switching experiments involving devices constructed within 13 NTs, the threshold bias for transitions from the "OFF" to "ON" state was found to vary between 0.8 to 6 V. Current versus voltage plots demonstrating the operation of four supermolecular switches realized within a NT are shown in Fig. 2(a). The voltages required for establishing an "ON" state in these four devices were found to be in the 0.8 to 2 V range. This variation in threshold bias can be attributed to differences in the intersegment gaps at each of the four devices. SEM imaging provides direct evidence for intershell displacements induced by electrostatic actuation. Figure 2(b) shows a switch in the "OFF" state with the gap clearly visible, while panel "c" shows the gap closed due to electromechanical actuation of the core shells resulting in an "ON" state.

The repeatability in performance of these devices was experimentally investigated by applying the excitation bias several times to a single device. For the device shown in Fig. 3(a), the "ON" state current in the first cycle reached a peak of 7.35 μA at 2.5 V. Beyond this bias, unexpected steplike decreases in current were observed. These current steps are similar to those previously observed during current driven evaporation of MWNT shells[14] and indicate a loss of outer NT shells. During the next cycle, the threshold bias for switching increased to 1.7 V (from 1.1 V in the first cycle) and the peak current reduced to 4.08 μA. Apart from current steps in the first cycle, this reduction in "ON" currents during the second cycle also points to increased device resistance associated with a lower number of shells. However, after the initial reduction in currents, the switching behavior was found to be stable and repeatable as seen in the overlapping plots for cycles 2 and 3. Information on other device and process failure modes can be found in Supplementary Online Information.[17]

Figure 3(b) represents the hysteresis plot of a device in which the voltage was first increased from 0 to 3 V and, then, decreased from 3 to 0 V. As can be seen from the measurement, it is evident that the device reaches the "ON" state at 1.8 V during the increasing voltage segment and returns to the "OFF" state at 1.2V during the decreasing voltage segment. This characteristic can be attributed to electrostatic

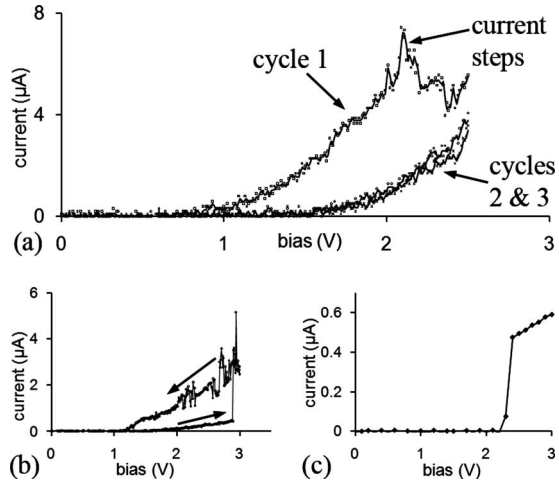

FIG. 3. Device repeatability and hysteresis measurements. (a) Evolution of I-V plots during three successive switching cycles. The steplike reduction in currents during the first cycle is attributed to the loss of outer NT shells. The behavior during the second and third cycles remains repeatable but with a lower "ON" current as compared to the first cycle. (b) Hysteresis behavior indicated by I-V plots of switches during the increasing and decreasing voltage cycles. It can be seen that the "OFF"-to-"ON" transition (1.8 V) occurs at a higher voltage as compared to the "ON"-to-"OFF" transition (1.2 V). (c) The only device that exhibited an Ohmic interface between NT segments in the "ON" state.

interactions between the inner shells of the two NT segments, which are a function of both the applied voltage as well as NT position. This component is significantly higher during the decreasing voltage segment (where the inner shells are in proximity at the initial state) as compared to the increasing voltage segment (where the inner shells are separated by the fabrication-defined gap of ~6–15 nm at the initial state).

Furthermore, the increase in current beyond the threshold voltage (without a steep step) is characteristic of tunneling transport at the intersegment interface, and indicates that the carbon atoms on opposing segments do not re-establish covalent bonds in the "ON" state. This behavior is different from the previous report on telescoping NEMS switches[13] in which the I-V curve exhibited a steplike increase at the threshold bias and the NT segments remained welded to each other after switching. In switches characterized as a part of our effort, this behavior occurred in only one device [Fig. 3(c)], with the rest exhibiting an I-V profile that indicates tunneling transport at the interface between NT segments during the "ON" state. This difference arises from the fact that we have characterized our devices primarily in air, and there was no inert ambient created by the flow of Argon, as was the case in Ref. 13. We believe that the difference in intersegment interface at contact arises from this variation in operating conditions within the two efforts.

We have presented a detailed overview of a low-power, electrostatically actuated NEMS switch based on bidirectional MWNT bearings. The investigation focused on the voltage requirement, repeatability, hysteresis and device failure modes. Further contributions of the work arise from the demonstration of multiple switches within a single MWNT supermolecule, paving the way for high densities.

The authors thank FIRST laboratory of ETH Zurich for technical support. This work was partially supported by the Swiss Nano-Tera Program and by the Swiss National Science Foundation (Grant No. 200021–117966).

[1]J. Cumings and A. Zettl, Science **289**, 602 (2000).
[2]M. F. Yu, B. I. Yakobson, and R. S. Ruoff, J. Phys. Chem. B **104**, 8764 (2000).
[3]A. M. Fennimore, T. D. Yuzvinsky, W. Q. Han, M. S. Fuhrer, J. Cumings, and A. Zettl, Nature (London) **424**, 408 (2003).
[4]B. Bourlon, D. C. Glattli, C. Miko, L. Forro, and A. Bachtold, Nano Lett. **4**, 709 (2004).
[5]L. X. Dong, B. J. Nelson, T. Fukuda, and F. Arai, IEEE Trans. Autom. Sci. Eng. **3**, 228 (2006).
[6]K. Jensen, C. Girit, W. Mickelson, and A. Zettl, Phys. Rev. Lett. **96**, 215503 (2006).
[7]S. J. Papadakis, A. R. Hall, P. A. Williams, L. Vicci, M. R. Falvo, R. Superfine, and S. Washburn, Phys. Rev. Lett. **93**, 146101 (2004).
[8]J. W. Kang and Q. Jiang, Nanotechnology **18**, 095705 (2007).
[9]Q. M. Yan, G. Zhou, S. G. Hao, J. Wu, and W. H. Duan, Appl. Phys. Lett. **88**, 173107 (2006).
[10]L. Maslov, Nanotechnology **17**, 2475 (2006).
[11]A. M. Popov, E. Bichoutskaia, Y. E. Lozovik, and A. S. Kulish, Phys. Status Solidi A **204**, 1911 (2007).
[12]A. S. Kulish, A. M. Popov, Y. E. Lozovik, and E. Bichoutskaia, Fullerenes, Nanotubes, Carbon Nanostruct. **16**, 340 (2008).
[13]V. V. Deshpande, H. Y. Chiu, H. W. C. Postma, C. Miko, L. Forro, and M. Bockrath, Nano Lett. **6**, 1092 (2006).
[14]A. Subramanian, L. X. Dong, J. Tharian, U. Sennhauser, and B. J. Nelson, Nanotechnology **18**, 075703 (2007).
[15]I. Yagi, K. Tsukagoshi, E. Watanabe, and Y. Aoyagi, Microelectron. Eng. **73–74**, 675 (2004).
[16]A. Subramanian, T.-Y. Choi, L. X. Dong, J. Tharian, U. Sennhauser, D. Poulikakos, and B. J. Nelson, Appl. Phys. A: Mater. Sci. Process. **89**, 133 (2007).
[17]See supplementary material at http://dx.doi.org/10.1063/1.3327514 for further information on device and process failure modes.